Photoexcitation and ionization in molecular fluorine: Stieltjes–Tchebycheff calculations in the static-exchange approximation

A. E. Orel and T. N. Rescigno

Theoretical Atomic and Molecular Physics Group, Lawrence Livermore Laboratory, University of California, Livermore, California 94550

B. V. McKoy

A. A. Noyes Laboratory of Chemical Physics, California Institute of Technology, Pasadena, California 91125

P. W. Langhoff

Department of Chemistry, [a] *Indiana University, Bloomington, Indiana 47405, Computational Chemistry Group, NASA-Ames Research Center, Moffett Field, California 94035, and Department of Aeronautics and Astronautics, Stanford University, Stanford, California 94305*
(Received 4 June 1979; accepted 24 September 1979)

Theoretical investigation of outer ($1\pi_g$, $1\pi_u$, $3\sigma_g$) and inner ($2\sigma_u$, $2\sigma_g$) valence-shell electronic photoexcitation and ionization cross sections in molecular fluorine are reported employing separated-channel static-exchange calculations and Stieltjes–Tchebycheff (S–T) moment-theory techniques. The discrete vertical electronic $1\pi_g$ excitation series are found to be in good agreement with recent spectral assignments and previously reported theoretical studies, and those for $1\pi_u$, $3\sigma_g$, $2\sigma_u$ and $2\sigma_g$ excitations are in general accord with position and intensity estimates based on quantum-defect analysis. Certain of the partial-channel photoionization cross sections in F_2 are seen to exhibit resonancelike features similar to those reported recently in related ST studies of photoionization in N_2, CO, and O_2. The resonances can be attributed to valencelike and pre-Rydberg diabatic states that cross the outer limbs of appropriate Rydberg series and corresponding ionic-state potential curves as functions of internuclear coordinate, giving rise to large continuum transition intensities at the ground-state equilibrium internuclear separation. In contrast to the situation in N_2, CO, and O_2, however, there is no evidence of a resonance like $\sigma \rightarrow \sigma^*$ feature in the $3\sigma_g \rightarrow k\sigma_u$ photoionization channel in F_2. Rather, this resonance in F_2 appears as a strong $N \rightarrow V_\sigma$ transition below the $3\sigma_g$ ionization threshold, and the corresponding partial-channel photoionization cross section is seen to be structureless. Although experimental studies of partial-channel photoionization cross sections are apparently unavailable for comparison, the calculations reported here should provide reliable approximations to the dipole excitation/ionization spectra in F_2, and are helpful in understanding and clarifying the dependences of photoionization spectra in light diatomic molecules on shell occupancy and equilibrium internuclear separation when compared with the results of previous studies of photoionization in N_2, CO, and O_2.

I. INTRODUCTION

A recent series of articles reports theoretical investigations of valence-shell photoexcitation and ionization cross sections in N_2, CO, and O_2 employing separated-channel static-exchange calculations and Stieltjes–Tchebycheff (ST) moment-theory techniques.[1–5] The calculated cross sections are found to be in generally good accord with corresponding discrete spectral measurements[6–8] and partial-channel photoionization studies,[9–19] suggesting that the static-exchange approximation is appropriate for investigations of valence-shell excitation–ionization spectra in light diatomic molecules provided realistic noncentral potentials are employed and the correct ionic parentages of the photoionization multiplets are included in the development in open-shell cases.[3,4] The reported theoretical and experimental partial-channel cross sections exhibit interesting resonancelike features that can be satisfactorily interpreted by extension of conventional molecular-orbital concepts to the photoionization continuum. Specifically, it is suggested that valencelike and pre-Rydberg diabatic states cross the outer limbs of appropriate Rydberg series and corresponding ionic-state potential curves as functions of the internuclear coordinate, and appear in the continua as photoionization resonances at the ground-state equilibrium separations. The resonance states assigned to the continuous photoionization spectra include the familiar $\sigma \rightarrow \sigma^*$ or V_σ charge-transfer states in N_2 and O_2 [$(3\sigma_g^{-1}\sigma_u 2p)\,^1\Sigma_u^+$], and in CO [$(5\sigma^{-1}\sigma^* 2p)\,^1\Sigma^+$], as well as states having an apparent atomic origin involving $3d$ orbitals. In order to further clarify the natures of these resonances, and to study their dependence on bond lengths and shell occupancies, it is desirable to perform additional calculations on appropriately chosen systems.

Molecular fluorine would seem to provide an appropriate system for comparative study. Although experimental photoionization cross sections are apparently unavailable, photoelectron spectra[20–22] and both experimental[23,24] and theoretical[25–29] studies of the discrete spectral region have been reported. Moreover, since the photoexcitation spectrum in F_2 includes a strong $3\sigma_g \rightarrow 3\sigma_u$ intravalence $N \rightarrow V_\sigma$ transition,[25–29] it is of par-

[a] Permanent address.

 0021-9606/80/021265-11$01.00

ticular interest to study the corresponding $3\sigma_g \rightarrow k\sigma_u$ photoionization continuum, which is expected to be relatively structureless on the basis of previously described interpretations of spectra in N_2, CO, and O_2.[1-4] In addition, because of the relatively long bond length and completely filled $1\pi_g$ shell in F_2, comparison of the spectrum with that of O_2 reported previously is expected to be illuminating.[3,4]

As in previously reported studies in this series,[1-4] canonical Hartree–Fock orbitals and Gaussian computational methods[30,31] are employed in constructing discrete excitation spectra and pseudospectral states for the ST analysis.[32-37] The resulting discrete excitation series are compared with spectral assignments and previously reported theoretical studies.[20-29] Although there is general agreement between the experimental and theoretical values for the $1\pi_g$ series, and the calculated higher-lying $1\pi_u$ and $3\sigma_g$ excitations are in accord with quantum-defect approximations, autoionizing line-shape calculations for the higher series are not reported, and so the intensities must be regarded as tentative in these cases. The calculated partial-channel photoionization cross sections are in general accord with the previously reported corresponding cross sections in O_2.[3,4] Specifically, $(1\pi_g^{-1}\pi_u 3d)^1\Sigma_u^+$, $(1\pi_g^{-1}\delta_u 3d)^1\Pi_u$, $(1\pi_u^{-1}\delta_g 3d)^1\Pi_u$, and $(3\sigma_g^{-1}\pi_u 3d)^1\Pi_u$ pre-Rydberg states apparently contribute to the $1\pi_g$, $1\pi_u$, and $3\sigma_g$ continua. There is no evidence, however, of a $\sigma \rightarrow \sigma^*$ resonance in the $3\sigma_g \rightarrow k\sigma_u$ photoionization cross section, in contrast to the situation in N_2, CO, and O_2.[1-5] Rather, as indicated above, this feature in F_2 appears as a strong $3\sigma_g \rightarrow 3\sigma_u$ intravalence $N \rightarrow V_\sigma$ transition below the $3\sigma_g^{-1}$ ionization threshold, and the corresponding $3\sigma_g \rightarrow k\sigma_u$ photoionization cross section is relatively structureless, an apparent consequence of the longer bond length in F_2 relative to those in N_2, CO, and O_2. This and other aspects of the F_2 cross sections are discussed and are contrasted and compared with the results of the previously reported studies in N_2, CO, and O_2.[1-5]

The general ST scheme is described briefly in Sec. II, and the specific calculations performed in F_2 are reported in Sec. III. In Sec. IV the calculated discrete and continuum spectra are presented, and some concluding remarks are made in Sec. V.

II. THEORETICAL APPROACH

The Stieltjes–Tchebycheff procedure and the separated-channel static-exchange approximation are described in considerable detail in previous publications.[1-5] Consequently, only a brief description of the general scheme is presented here.

A ground-state Hartree–Fock function is constructed near the equilibrium molecular geometry employing Gaussian basis orbitals and appropriate computational methodology.[30,31] Noncentral static-exchange potentials are constructed from the resulting canonical orbitals using many-electron wave functions of correct symmetry for each orbital excitation considered, and corresponding one-electron Schrödinger equations are formed for the calculation of excitation spectra. These equations are solved variationally employing significantly larger basis sets than that employed in constructing the ground-state Hartree–Fock function.[31] The one-electron eigenvalues obtained that are below the occupied-orbital ionization potential, and the corresponding one-electron orbitals, provide so-called improved-virtual-orbital (IVO) approximations to the appropriate discrete or autoionizing valence and Rydberg states.[38] Those eigenvalues above the ionization potential, and their corresponding orbitals, provide pseudospectra for the Stieltjes–Tchebycheff moment analysis, from which the appropriate static-exchange photoionization cross sections are obtained.

The ST approach employs the pseudospectrum of discrete transition frequencies and oscillator strengths calculated in the present study as indicated above in a smoothing procedure in which a continuous approximation to the underlying photoionization cross section is obtained.[5] Conventional spectral power moments, which are convergent in the L^2 pseudospectrum of energies and strengths, are generally regarded as intermediaries in the smoothing procedure, providing a basis for establishing the convergence of the overall approach.[5] In actual calculations, however, the power moments are avoided, and a highly stable computational algorithm is employed in constructing so-called recurrence coefficients and moment-theory spectra of (principal) frequency points and weights directly from the quantum mechanically determined pseudospectrum.[36] The moment-theory spectra exhibit useful properties which the original pseudospectrum does not exhibit, and, in particular, provide bounds on the cumulative oscillator-strength distribution.[5] The latter can be differentiated in a variety of ways to provide a final expression for the photoionization cross section. Stieltjes derivatives of various orders are generally employed to obtain a first approximation to the continuous cross section,[32-34] and to establish the range of convergence of the variationally calculated recurrence coefficients. Tchebycheff derivatives and appropriate recurrence-coefficient extension procedures can then be used to construct a continuous approximation to the cross section.[35-37] In addition, specific analytic forms fit to the cumulative Stieltjes histograms provide expressions convenient for differentiation.[34] Polynomials in $1/\epsilon$ are particularly convenient, and are employed in the present development. Previous investigations indicate the method is highly reliable when the ground-state wave function is satisfactory and the quantum-mechanical pseudostate calculation provides sufficient information to describe the underlying continuous spectrum.[1-5]

III. MOLECULAR FLUORINE STATIC-EXCHANGE CALCULATIONS

The ground state of F_2 at the equilibrium internuclear separation ($R_e = 2.68\,a_0$) can be approximated by a single Slater determinant comprised of canonical Hartree–Fock orbitals in the form

$$(1\sigma_g^2 1\sigma_u^2 2\sigma_g^2 2\sigma_u^2 3\sigma_g^2 1\pi_u^4 1\pi_g^4)\, X\,^1\Sigma_g^+ . \quad (1)$$

Recent configuration-interaction calculations indicate that the next largest term in the wave function is given by the $3\sigma_g^2 \rightarrow 3\sigma_u^2$ configuration, which contributes approx-

TABLE I. Static-exchange potentials and multiplicity factors in molecular fluorine.[a,b]

γ \ i	$2\sigma_g$	$2\sigma_u$	$3\sigma_g$	$1\pi_u^x$	$1\pi_u^y$	$1\pi_g^x$	$1\pi_g^y$	μ_γ[c]
$2\sigma_g \rightarrow k\sigma_u$	$\frac{1}{2}/-1$	1/1	1/1	1/1	1/1	1/1	1/1	2
$\rightarrow k\pi_u^x$	$\frac{1}{2}/-1$	1/1	1/1	1/1	1/1	1/1	1/1	4
$2\sigma_u \rightarrow k\sigma_g$	1/1	$\frac{1}{2}/-1$	1/1	1/1	1/1	1/1	1/1	2
$\rightarrow k\pi_g^x$	1/1	$\frac{1}{2}/-1$	1/1	1/1	1/1	1/1	1/1	4
$3\sigma_g \rightarrow k\sigma_u$	1/1	1/1	$\frac{1}{2}/-1$	1/1	1/1	1/1	1/1	2
$\rightarrow k\pi_u^x$	1/1	1/1	$\frac{1}{2}/-1$	1/1	1/1	1/1	1/1	4
$1\pi_u^x \rightarrow k\sigma_g$	1/1	1/1	1/1	$\frac{1}{2}/-1$	$\frac{1}{2}/-1$	1/1	1/1	4
$\rightarrow k\pi_g^x$	1/1	1/1	1/1	$\frac{1}{4}/-3$	$\frac{5}{4}/5$	1/1	1/1	4
$\rightarrow k\delta_g^{xy}$	1/1	1/1	1/1	$\frac{3}{4}/1$	$\frac{3}{4}/1$	1/1	1/1	8
$1\pi_g^x \rightarrow k\sigma_u$	1/1	1/1	1/1	1/1	1/1	$\frac{1}{2}/-1$	$\frac{1}{2}/-1$	4
$\rightarrow k\pi_u^x$	1/1	1/1	1/1	1/1	1/1	$\frac{1}{4}/-3$	$\frac{5}{4}/5$	4
$\rightarrow k\delta_u^{xy}$	1/1	1/1	1/1	1/1	1/1	$\frac{3}{4}/1$	$\frac{3}{4}/1$	8

[a]Values of the coefficients a_i^γ/b_i^γ appearing in the potential of Eq. (5).
[b]The $1\sigma_g$ and $1\sigma_u$ orbitals remain doubly occupied throughout, and, consequently, $a_i^\gamma = 1$, $b_i^\gamma = 1$ in these cases.
[c]Multiplicity factors of Eq. (7c).

imately 4% to the total structure at the equilibrium internuclear separation.[29] Although larger contributions are expected with increasing nuclear separation,[27] Eq. (1) is employed here since attention is restricted to vertical excitation and ionization at the ground-state equilibrium internuclear separation. A $(10s, 5p, 1d)/[3s, 2p, 1d]$ contracted Gaussian basis set is employed in the calculations, giving a total self-consistent-field (SCF) energy of -198.734 a.u.,[31] compared with the HF limit of -198.768 a.u.[25] The occupied canonical orbitals have been described in considerable detail elsewhere,[39] and need not be explicitly characterized here.

One-electron excitation and ionization of the outer and inner valence orbitals of Eq. (1) gives many-electron eigenstates that can be written symbolically in the forms

$$(1\pi_g^{-1} k\sigma_u)\,{}^1\Pi_u, \quad (1\pi_g^{-1} k\pi_u)\,{}^1\Sigma_u^+, \quad (1\pi_g^{-1} k\delta_u)\,{}^1\Pi_u\ ; \tag{2a}$$

$$(1\pi_u^{-1} k\sigma_g)\,{}^1\Pi_u, \quad (1\pi_u^{-1} k\pi_g)\,{}^1\Sigma_u^+, \quad (1\pi_u^{-1} k\delta_g)\,{}^1\Pi_u\ ; \tag{2b}$$

$$(3\sigma_g^{-1} k\sigma_u)\,{}^1\Sigma_u^+, \quad (3\sigma_g^{-1} k\pi_u)\,{}^1\Pi_u\ ; \tag{2c}$$

$$(2\sigma_u^{-1} k\sigma_g)\,{}^1\Sigma_u^+, \quad (2\sigma_u^{-1}, k\pi_g)\,{}^1\Pi_u\ ; \tag{2d}$$

$$(2\sigma_g^{-1} k\sigma_u)\,{}^1\Sigma_u^+, \quad (2\sigma_g^{-1}, k\pi_u)\,{}^1\Pi_u\ . \tag{2e}$$

It is expected that single-hole states will provide adequate descriptions of the cores produced upon ionization of the outer valence $1\pi_g$, $1\pi_u$, and $3\sigma_g$ orbitals at the equilibrium internuclear separation,[26-29] but that additional (two-hole–one-particle) states may be required for correct treatments of the ionic states produced upon ionization of inner-valence $2\sigma_u$ and $2\sigma_g$ orbitals.[40] The latter aspects of inner-valence-shell photoionization are treated separately in a subsequent paper.

In each of the cases of Eqs. (2), many-electron wave functions of correct symmetry are used in constructing appropriate static-exchange potentials, resulting in one-electron Schrödinger equations for the final-state orbitals of the form

$$(h_\gamma - \epsilon)\phi_{\gamma,\epsilon} = 0\ , \tag{3}$$

where ϵ can take on discrete or continuous values and γ is a channel label. The Hamiltonians are of the form

$$h_\gamma = T + V + V_\gamma\ , \tag{4}$$

where T and V are the kinetic-energy and nuclear-potential-energy operators, respectively, and the static-exchange potential V_γ for the channel γ can be written in terms of the customary Coulomb and exchange operators in the form[1-5]

$$V_\gamma = \sum_i \left(2a_i^\gamma \hat{J}_i - b_i^\gamma \hat{K}_i\right)\ . \tag{5}$$

The coefficients a_i^γ and b_i^γ for all cases treated here are given in Table I.

Variational solutions of Eqs. (3) are obtained in the form

$$\langle \tilde{\phi}_{\gamma,i} | h_\gamma | \tilde{\phi}_{\gamma,j} \rangle = \tilde{\epsilon}_{\gamma,i}\delta_{ij}\ , \tag{6a}$$

$$\langle \tilde{\phi}_{\gamma,i} | \tilde{\phi}_{\gamma,j} \rangle = \delta_{ij}, \quad i,j = 1,N \tag{6b}$$

employing expansions in a virtual space orthogonal to the occupied canonical orbitals, constructed using the ground-state basis set and the supplemental orbitals shown in Table II. Although virtual spaces of relatively large dimensions are employed ($17\sigma_g$, $18\sigma_u$, $16\pi_g$, $16\pi_u$, $14\delta_g$, $10\delta_u$), possible deficiencies in the supplemental basis set of Table II are indicated at appropriate points in the subsequent text.

One-electron transition energies and oscillator strengths are obtained from the pseudospectra of Eqs. (6) in the form

TABLE II. Supplemental Gaussian basis functions used in F_2 static-exchange calculations.[a]

Location	Type	Number	Exponent range[b]
		σ_g/σ_u	
F/F	s/s	2/2	0.2–0.1/0.2–0.1
F/F	p_z/p_z	2/2	0.16–0.1/0.16–0.1
c.m./c.m.	s/p_z	10/10	0.3–0.0015/0.3–0.0015
		π_g/π_u	
F/F	p_x/p_x, d_{xz}	4/4, 8	1.0–0.1/1.0–0.1
c.m./c.m.	d_{xz}/p_x, p_x	10/10,5	0.3–0.0015/0.3–0.0015
		δ_g/δ_u	
F/F	d_{xy}/d_{xy}	4/10	1.0–0.1/3.0–0.009
c.m./c.m.	d_{xy}/···	10/···	0.3–0.0015/···

[a]Supplemental basis functions employed, in addition to the $(10s, 5p, 1d)/[3s, 2p, 1d]$ valence basis [Ref. 31], in solution of the static-exchange equations [Eqs. (3)–(6)]. Two separate π_u basis sets are employed, as is discussed further in the text.
[b]A geometric-series variation is employed in the indicated ranges.

$$\tilde{\epsilon}_i^{\gamma} = \epsilon_{\gamma} + \tilde{\epsilon}_{\gamma,i} \ , \tag{7a}$$

$$\tilde{f}_i^{\gamma} = \tfrac{2}{3}\tilde{\epsilon}_i^{\gamma} |\langle \tilde{\phi}_{\gamma,i} | \mu | \phi_{\gamma} \rangle|^2 \ , \tag{7b}$$

where ϕ_γ is the appropriate occupied orbital and ϵ_γ is the experimentally determined vertical ionization potential.[20–22] Use of the experimental ϵ_γ, rather than the Koopmans value, ensures that the various discrete series converge on the appropriate thresholds, and allows in some measure for the effects of core relaxation. The one-electron oscillator strengths of Eq. (7b) must be multiplied by appropriate factors to determine the correct many-electron multiplet transition strengths,[41–43] resulting in total pseudospectral f numbers of the form

$$\tilde{F}_i^{\gamma} = \mu_{\gamma} \tilde{f}_i^{\gamma} \ . \tag{7c}$$

The multiplicity factors μ_γ are conveniently tabulated in Table I. Finally, the many-electron pseudospectra of transitions energies and strengths are employed in the ST construction of photoexcitation and ionization cross sections.

IV. PHOTOEXCITATION AND IONIZATION CROSS SECTIONS IN MOLECULAR FLUORINE

In Tables III–V and Figs. 1–5 are shown the discrete excitation series and photoionization cross sections obtained from the present calculations, in comparison with previous theoretical results,[26–29] and available experimental data.[20–24] Although some of the discrete transitions have been assigned and related calculations performed, and photoelectron spectra have been measured, experimental photoionization cross sections in F_2 are apparently unavailable. Consequently, it will be helpful to contrast and compare the present results with the previously reported photoionization studies in N_2, CO, and particularly O_2, in which cases there are corresponding experimental studies to lend support to the theoretical predictions.[1–19] In this connection it is convenient to regard the dipole excitation and ionization spectra in diatomic molecules as arising from transitions between occupied canonical orbitals and valencelike and Rydberg virtual orbitals that appear in both discrete and continuous spectral intervals.[1–5] In N_2, CO, and O_2 the $3\sigma_g^{-1}$, $5\sigma^{-1}$, and $3\sigma_g^{-1}$ cross sections, respectively, are dominated by broad $\sigma \rightarrow k\sigma^*$ resonancelike features, conveniently regarded as consequences of $\sigma_u 2p/\sigma^* 2p$ valencelike virtual orbitals appearing in the photoionization continua, rather than in the discrete $np\sigma_u/np\sigma$ spectra, which later are comprised of Rydberg transitions only. The $1\pi_u^{-1}$, $1\pi^{-1}$ and $1\pi_u^{-1}$ cross sections in N_2, CO, and O_2, respectively, are dominated by strong $\pi \rightarrow \pi^*$ discrete (autoionizing) transitions and broad $\pi_u \rightarrow k\delta_g/\pi \rightarrow k\delta$ photoionization resonances. The latter are conveniently attributed to contributions from atom-centered "pre-Rydberg" $3d$ atomic orbitals.[44] Similarly, the $1\pi_g^{-1}$ cross section in O_2 has broad $1\pi_g \rightarrow k\pi_u$ and $k\delta_u$ photoionization resonances attributed to contributions from $3d$ pre-Rydberg atomic-oxygen orbitals.[3,4]

Many of the features in the N_2, CO, and O_2 spectra also appear in the F_2 excitation and ionization cross sections described below. However, the $\pi \rightarrow \pi^*$ transition is, of course, not present in F_2 since the $1\pi_g$ shell is closed, and the $3\sigma_g^{-1}$ cross section is found to be dominated by a strong $3\sigma_g \rightarrow 3\sigma_u$ or $N \rightarrow V_\sigma$ intravalence transition below the ionization threshold, rather than by a $3\sigma_g \rightarrow k\sigma_u$ photoionization resonance, as indicated above.

A. $1\pi_g$ spectra (IP = 15.8 eV)

In Table III and Fig. 1 are shown the $1\pi_g^{-1}$ discrete and continuum spectra in F_2, respectively, obtained from the present calculations. Also shown in the table are spectral assignments and the results of previous calculations.[23,24,26–29]

The $1\pi_g \rightarrow np\sigma_u$ excitations are evidently comprised of a low-lying intravalence $1\pi_g \rightarrow \sigma_u 2p$ transition, and a

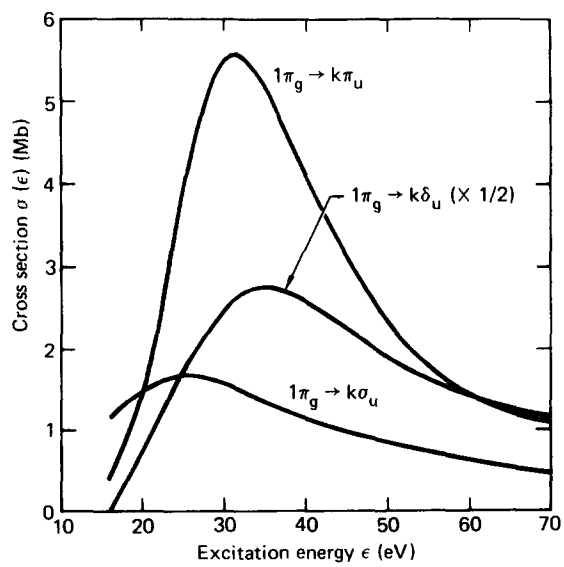

FIG. 1. Partial-channel cross sections for $1\pi_g \rightarrow k\sigma_u$, $k\pi_u$, and $k\delta_u$ photoionization in F_2 obtained from the development of Eqs. (1)–(7) and the Stieltjes–Tchebycheff technique. 1 Mb $= 10^{-18}$ cm^2.

TABLE III. $1\pi_g$ excitation spectra in F_2 (IP = 15.8 eV).

Present results[a] [energy (eV)/f number]	Experimental values[b] [energy (eV)/intensity]	Previous calculations[c] [energy (eV)/f number]
	$(1\pi_g)^1\Sigma_g^+ - (np\sigma_u)^1\Pi_u$	
2.85/0.00042	~4.36/continuous	$3.91/4\times10^{-5}$
13.32/0.01468	13.35/medium	13.01/0.0226
14.63/0.00545	14.49/	14.53/
15.12/0.00257	14.98/	15.05
15.38/0.00218	15.23/	···
	$(1\pi_g)^1\Sigma_g^+ - (np\pi_u)^1\Sigma_u^+$	
13.35/0.00100	13.15/medium	13.38/0.073
14.63/0.00026	14.42/	14.66/
15.12/0.00010	14.95/	15.15/
15.38/0.00008	15.22/	···
	$(1\pi_g)^1\Sigma_g^+ - (n\delta_u)^1\Pi_u$	
15.03/0.00025	14.29/···	15.01/···
15.85/0.···	14.95/	15.38/

[a]Values obtained from Eqs. (3)–(7) employing the basis sets described in Sec. III and Table II. The indicated series are made to converge on the experimentally determined ionic state, and the f numbers indicated correspond to total line strengths, as discussed in the text.

[b]Spectral assignments taken from J. L. Gole and J. L. Margrave, J. Mol. Spectrosc. **43**, 65 (1972). See also E. A. Colbourn, M. Dagenais, A. E. Douglas, and J. W. Raymonds, Can. J. Phys. **54**, 1343 (1976), and references cited therein. The approximate position (4.36 eV) of the $1\pi_g \rightarrow \sigma_u 2p$ repulsive valence transition is taken from G. Herzberg, *Spectra of Diatomic Molecules* (Van Nostrand, New York, 1950). The values cited for the $1\pi_g \rightarrow n\delta_u$ series are Rydberg estimates using a quantum defect $\delta = 0$ for $n = 3$ and 4.

[c]Energies taken from the two-configuration IVO calculations of D. Demoulin and M. Jungen, Chem. Phys. **16**, 311 (1976). See also, S. Fraga and B. Ransil, J. Chem. Phys. **35**, 669 (1961); E. Kasseckert and B. Wirsam, Z. Naturforsch. **299**, 1425 (1974); P. J. Hay and D. C. Cartwright, Chem. Phys. Lett. **41**, 80 (1976); **42**, 398 (1976); T. N. Rescigno, C. F. Bender, and B. V. McKoy, Chem. Phys. Lett. **45**, 307 (1977); D. C. Cartwright and P. J. Hay, J. Chem. Phys. **70**, 3191 (1979). The f numbers are taken from the calculations of P. J. Hay and D. C. Cartwright cited in the foregoing.

Rydberg series ($n = 3, 4, 5, \ldots$) with quantum defect $\delta \cong 0.65$. The former is in general accord with but somewhat lower than the vertical position of the observed transition.[42] The latter is an estimate based on the maximum in the absorption continuum which results from the repulsive behavior of the final state. The two-configuration IVO[27] and configuration-interaction[29] calculations for this state are in somewhat better agreement with the experimental position, presumably as a consequence of including the $3\sigma_u^2$ configuration in the ground-state, which apparently gives rise to a significant $(3\sigma_u^2 3\sigma_g 1\pi_u)$ contribution to the $1\,^1\Pi_u$ state.[29] The $1\pi_g \rightarrow np\sigma_u$ Rydberg series of Table III, which appears at significantly higher energy than the $1\pi_g \rightarrow \sigma_u 2p$ intravalence transition, is in very good agreement with the spectral assignments[23,24] and previously reported two-configuration IVO calculations.[27] In contrast to the situation in F_2, the $(1\pi_g^{-1}\sigma_u 2p)\,^3\Pi_u$ state in O_2 undergoes strong interaction with the $(1\pi_g^{-1} np\sigma_u)\,^3\Pi_u$ Rydberg series, the various crossings occurring approximately at the ground-state equilibrium internuclear separation.[45] Presumably the $(1\pi_g^{-1}\sigma_u 2p)\,^1\Pi_u$ state in F_2 is much lower in excitation energy than is the $(1\pi_g^{-1}\sigma_u 2p)\,^3\Pi_u$ state in O_2 as a consequence of the longer bond length in the former ($2.68\,a_0$ vs $2.28\,a_0$), providing a larger effective molecular box for the $\sigma_u 2p$ orbital in F_2. However, referring to Fig. 1, the $1\pi_g \rightarrow k\sigma_u$ photoionization cross section in F_2, which is evidently weak and broad, is seen to bear strong similarity to the corresponding profile in O_2.[3,4]

The $1\pi_g \rightarrow np\pi_u$ excitations in Table III evidently comprise a Rydberg series ($n = 3, 4, \ldots$) with $\delta \cong 0.65$, the positions of which are in very good accord with both experimental assignments and previous calculations.[23,24,27] Evidently, the previously reported f number for the resonance transition in this series is significantly larger than the present result, and also larger than estimates based on the Coulomb approximation (not shown). The corresponding $1\pi_g \rightarrow k\pi_u$ photoionization cross section of Fig. 1 shows a strong resonance feature centered at ~32 eV, which can be attributed to contributions from atomic-fluorine pre-Rydberg $3p$ and $3d$ orbitals.[44] To test the sensitivity of this strong feature to basis set, the 10 p_x functions at the c.m. in this symmetry (Table II) were reduced to 5 p_x functions and eight additional d_{xz} functions were added to the F centers. The $1\pi_g \rightarrow k\pi_u$ cross section so obtained was indistinguishable from that of Fig. 1, although the $np\pi_u$ Rydberg series was poorly reproduced in this basis. The corresponding $1\pi_g \rightarrow k\pi_u$ cross section in O_2 is remarkably similar to that found in F_2, although smaller by an appropriate factor of 2 for the half-filled $1\pi_g$ shell, verifying to some extent the existence of the strong resonance.[3,4] As in the case of O_2, the resonance feature in the $1\pi_g \rightarrow k\pi_u$ cross section of Fig. 1 can presumably be attributed to a pre-Rydberg diabatic $(1\pi_g^{-1}\pi_u 3d)\,^1\Sigma_u^+$ state that crossses the outer limbs of the $np\pi_u$ Rydberg series and corresponding $X\,^2\Pi_g$ ionic-state-potential curve as a function of internuclear distance, appearing in the continuum at the ground-state equilibrium internuclear separation. Although it is clear from the use of two distinct basis sets in this case (Table II) that both p- and d-type atomic-oxygen functions can be employed in constructing the pertinent $k\pi_u$ resonance orbitals, the $(1\pi_g^{-1}\pi_u 3d)\,^1\Sigma_u^+$ assignment is preferred since this state presumably correlates with the strongly allowed $(2p^{-1}3d)\,^2D^e$ atomic-fluorine state in the separated-atom limit.[46] By contrast, a $(1\pi_g^{-1}\pi_u 3p)\,^1\Sigma_u^+$ configurational state would be dipole forbidden in the separated-atom limit $[(2p^{-1}3p)\,^2P^0]$, although a precise assignment can be made only by examination of the appropriate diabatic states.

Finally, only two discrete $1\pi_g \rightarrow n\delta_u$ transitions in F_2 are obtained employing the basis set of Table II, the lowest of which is seen to be in good accord with the previously reported two-configuration IVO results.[27] This transition is significantly higher than the Rydberg estimate using a quantum defect $\delta = 0$ also shown in the table, suggesting that $3d$ atomic-fluorine orbitals do not contribute significantly to the $1\pi_g \rightarrow n\delta_u$ discrete excitation series. Rather, the $1\pi_g \rightarrow k\delta_u$ photoionization cross section of Fig. 1 shows a strong resonance feature centered at ~35 eV which can be attributed to $3d$ pre-Rydberg atomic orbitals.[44] As in the case of the $(1\pi_g^{-1}\pi_u 3d)\,^1\Sigma_u^+$ resonance discussed above, a $(1\pi_g^{-1}\delta_u 3d)\,^1\Pi_u$

TABLE IV. $1\pi_u$ (IP = 18.8 eV) and $3\sigma_g$ (IP = 21.0 eV) excitation spectra in F_2.

Present results[a] [energy (eV)/f number]	Quantum-defect estimates[b] [energy (eV)/f number]	Present results[a] [energy (eV)/f number]	Quantum-defect estimates[b,c] [energy (eV)/f number]
$(1\pi_u)\,^1\Sigma_g^+ \rightarrow (ns\sigma_g)\,^1\Pi_u$		$(3\sigma_g)\,^1\Sigma_g^+ \rightarrow (np\sigma_u)\,^1\Sigma_u^+$	
15.03/0.0935	15.03/0.1084	16.95/1.1108	16.87, 17.22, 18.00/···
17.18/0.0301	17.18/0.0305	19.12/0.2735	19.12/0.000 63
17.90/0.0133	17.90/0.0125	19.98/0.0798	20.00/0.000 25
18.23/0.0080	18.23/0.0063	20.37/0.0328	20.38/0.000 12
18.60/···	18.41/0.0036	20.63/···	20.58/0.000 17
$(1\pi_u)\,^1\Sigma_g^+ \rightarrow (nd\pi_g)\,^1\Sigma_u^+$		$(3\sigma_g)\,^1\Sigma_g^+ \rightarrow (np\pi_u)\,^1\Pi_u$	
17.32/0.001 23	17.29/0.001 84	18.41/0.001 356	18.41/0.001 03
17.97/0.000 64	17.95/0.000 77	19.75/0.000 309	19.74/0.000 34
18.27/0.000 36	18.26/0.000 44	20.27/0.000 113	20.26/0.000 16
18.51/···	18.42/0.000 23	20.53/0.000 076	20.51/0.000 08
		20.96/···	20.66/0.000 05
$(1\pi_u)\,^1\Sigma_g^+ \rightarrow (nd\delta_g)\,^1\Pi_u$			
17.35/0.0269	17.29/0.0275		
17.99/0.0159	17.95/0.0116		
18.29/0.0094	18.26/0.0060		
18.66/···	18.42/0.0034		

[a] As in Table III.

[b] Quantum-defect estimates obtained from the Rydberg formula and the Coulomb approximation to f numbers at threshold [$f_n \sim g(\epsilon_t)/(n-\delta)^3$] of A. Burgess and M. J. Seaton [Mon. Not. R. Astron. Soc. 120, 121 (1960)], using quantum defects of $\delta = 1.1$, 0.0, 0.0, 0.31, and 0.71 for the $ns\sigma_g$, $nd\pi_g$, $nd\delta_g$, $np\sigma_u$, and $np\pi_u$ ($n = 3, 4, \ldots$) excitations, respectively, and photoionization oscillator-strength densities at threshold [$g(\epsilon_t)$ in a.u.] of Figs. 2 and 3.

[c] Previous estimates of the vertical position of the $(3\sigma_v^{-1}\,\sigma_u 2p)\,^1\Sigma_u^+ V_\sigma$ state are given by the two-configuration IVO calculations of D. Demoulin and M. Jungen, [Chem. Phys. 16, 311 (1976)] (16.87 eV), the RPA calculations of T. N. Rescigno, C. F. Bender, and B. V. McKoy [Chem. Phys. Lett. 45, 307 (1977)] (17.22 eV), and the CI calculations of C. F. Bender (private communication) (18.00 eV).

assignment is suggested in this case, although appropriate diabatic state calculations are clearly required for a precise assignment. Nevertheless, it is satisfying that these two strong resonance features are centered at approximately the same position in the photoionization continuum. The $1\pi_g \rightarrow k\delta_u$ profile of Fig. 1 is in rather good accord with the corresponding result in O_2.[3,4] Indeed, with the exception of an overall factor of 2 corresponding to orbital occupancy, the results of Fig. 1 are remarkably similar to those obtained previously in O_2. Although basis-set refinements will presumably result in quantitative changes in the $1\pi_g^{-1}$ spectra of Table III and Fig. 1, particularly in the discrete f numbers, it is highly unlikely that significant qualitative changes will result from such more elaborate calculations.

B. $1\pi_u$ spectra (IP = 18.8 eV)

In Table IV and Fig. 2 are shown the $1\pi_u^{-1}$ discrete and continuum spectra in F_2 obtained from the present calculations. Although there are few experimental and previous theoretical values for comparison in this case, the general behaviors of the spectra are in good accord with quantum-defect estimates in the discrete region, and with previously reported corresponding photoionization studies in N_2, CO, and O_2 in the continuum.[1-5]

The $1\pi_u \rightarrow ns\sigma_g$ excitations of Table IV are seen to form a strong Rydberg series ($n = 3, 4, \ldots$) in very good accord with the quantum-defect estimates using $\delta \cong 1.1$, and in accord with the corresponding results in N_2, CO, and O_2.[1-4] Both $ns\sigma$ and $np\sigma$ Rydberg series are of course present in the CO calculations.[2] Moreover, the associated $1\pi_u \rightarrow k\sigma_g$ photoionization cross section in Fig. 2 is monotonically decreasing from threshold, in excellent agreement with the previously reported N_2, CO, and O_2 results.[1-4] In the case of O_2, however, multiplet effects associated with the open $1\pi_g$ shell fur-

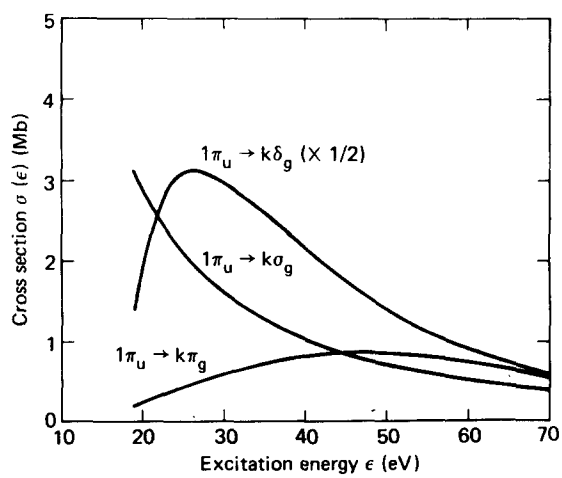

FIG. 2. As in Fig. 1, for $1\pi_u \rightarrow k\sigma_g$, $k\pi_g$, and $k\delta_g$ photoionization.

ther split the orbital photoionization cross sections into four separate electronic channels.[3,4]

The $1\pi_u \rightarrow nd\pi_g$ excitations of Table IV evidently form a Rydberg series in good accord with the quantum-defect estimates ($\delta = 0$). In contrast to the situation in N_2, CO, and O_2,[1-4] there is, of course, no strong $\pi \rightarrow \pi^*$ transition in F_2, since the $1\pi_g$ shell is closed in this case. This circumstance is important in connection with the $1\pi_u \rightarrow k\pi_g$ photoionization cross section of Fig. 2, which is seen to be broad and flat and highly similar to that in O_2.[3,4] By contrast, the static-exchange $1\pi_u \rightarrow k\pi_g$ and $1\pi \rightarrow k\pi$ photoionization cross sections in N_2 and CO, respectively, are apparently significantly perturbed by the presence of strong $\pi \rightarrow \pi^*$ transitions in the discrete spectral regions.[1,2] Reanalysis of the N_2 and CO photoionization spectra indicates the profiles in these cases are highly sensitive to the nature of the molecular potential employed, and to the presence of a compact π^* component in the basis set.[47] In the case of O_2, a virtual $k\pi_g$ spectrum explicitly orthogonalized to the occupied $1\pi_g$ orbital was employed in the calculations,[3,4] whereas this procedure was not employed in the N_2 and CO calculations.[1,2] When appropriate projection techniques are also used in the N_2 and CO calculations, $1\pi_u \rightarrow k\pi_g$ and $1\pi \rightarrow k\pi$ cross sections similar to the $1\pi_u \rightarrow k\pi_g$ cross sections in O_2 and F_2 are obtained.[47]

Finally, the $1\pi_u \rightarrow nd\delta_g$ discrete excitations are seen to be in general accord with the quantum-defect estimates ($\delta = 0$), and the $1\pi_u \rightarrow k\delta_g$ photoionization cross section of Fig. 2 shows a strong resonance feature centered at ~ 25 eV, in good agreement with the corresponding profiles in N_2, CO, and O_2.[1-5] As in these previously studied cases, the resonance in the $1\pi_u \rightarrow k\delta_g$ profile of Fig. 2 is assigned to a $(1\pi_u^{-1}\delta_g 3d)\,^1\Pi_u$ pre-Rydberg diabatic contribution corresponding to the strongly allowed $(2p^{-1}\,3d)\,^2D^e$ atomic-fluorine state in the separated-atom limit.

The three orbital photoionization profiles of Fig. 2 are highly similar to the previously reported results in O_2,[3,4] and to those in N_2 and CO when appropriate projection techniques are used to localize the $\pi \rightarrow \pi^*$ contribution in these cases,[47] and should be generally invariant to basis-set refinements.

C. $3\sigma_g$ spectra (IP = 21.0 eV)

In Table IV and Fig. 3 are shown the discrete and continuum spectra for $3\sigma_g$ excitation and ionization in F_2, respectively, obtained from the present calculations.

The calculated $3\sigma_g \rightarrow n\sigma_u$ excitations are evidently comprised of a strong $3\sigma_g \rightarrow \sigma_u 2p$ intravalence transition, and an $np\sigma_u$ Rydberg series ($n = 3, 4, 5, \ldots$) the positions of which are in very good accord with quantum-defect estimates obtained using a significantly perturbed defect ($\delta \cong 0.31$). Moreover, the intensities of the Rydberg-series members differ significantly from Coulomb estimates obtained using the threshold cross sectional value of the solid curve in Fig. 3, discussed further below. The position of the intravalence transition is in good agreement with earlier two-configuration IVO calculations (16.87 eV),[27] random-phase-approximation (RPA) calculations (17.22 eV),[28] and recent valence-basis configuration-interaction (CI) calculations (18.00 eV).[29] However, the theoretically determined f number of Table IV in this case is presumably a considerable overestimate, a view supported in some measure by the RPA and CI calculations, which indicate intensity sharing between the $(3\sigma_g^{-1}\sigma_u 2p)\,^1\Sigma_u^+$ and $(1\pi_g^{-1}3p\pi_u)\,^1\Sigma_u^+$ configurational states in this case. Moreover, the intravalence state evidently perturbs the $3\sigma_g \rightarrow np\sigma_u$ Rydberg series significantly, since a quantum defect of $\delta \cong 0.7$ is expected,[48] and the intensities are unreasonably large, differing considerably from the Coulomb estimates, as indicated above. As a consequence of this perturbation, the very rapid rise in the $3\sigma_g \rightarrow k\sigma_u$ photoionization cross section of Fig. 3 should be regarded as spurious, due to contributions from the valence $\sigma_u 2p$ portion of the basis set. When these spurious contributions are deleted from the ST analysis, the resulting $3\sigma_g \rightarrow k\sigma_u$ photoionization cross section in F_2, shown as a solid line in Fig. 3, is broad and quite weak. A somewhat related situation obtains in the $1\pi_u \rightarrow k\pi_g$ photoionization cross section in N_2, which is spuriously perturbed in the static-exchange approximation by the $1\pi_u \rightarrow 1\pi_g$ intravalence transition.[1] In this case a simple projection procedure is found to remove the spurious perturbation, and to provide a cross section in accord with observation.[47] Consequently, in order to substantiate the perturbation of the $3\sigma_g \rightarrow n\sigma_u/k\sigma_u$ cross section in F_2 by the $\sigma_u 2p$ orbital a separate calculation was performed employing a $k\sigma_u$ basis explicitly orthogonalized to the $\sigma_u 2p$ orbital obtained from a $(3\sigma_g^{-1}\sigma_u 2p)\,^3\Sigma_u^+$ state calculation. The resulting Rydberg series was found to be weak, in accord with expectations, and the $3\sigma_g \rightarrow k\sigma_u$ photoionization cross section was found to be in excellent agreement with the corresponding solid curve shown in Fig. 3.

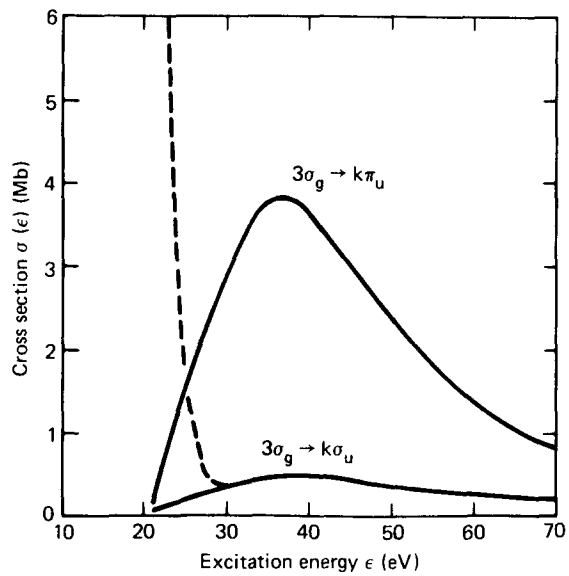

FIG. 3. As in Fig. 1, for $3\sigma_g \rightarrow k\sigma_u$ and $k\pi_u$ photoionization. The dotted line indicates a spurious contribution arising from perturbation of the $3\sigma_g \rightarrow np\sigma_u$ Rydberg series by the $3\sigma_g \rightarrow \sigma_u 2p$ intravalence transition, as is discussed in the text.

TABLE V. $2\sigma_u$ (IP = 40.8 eV) and $2\sigma_g$ (IP = 47.9 eV) excitation spectra in F_2.

Present results[a] [energy (eV)/f number]	Quantum-defect estimates[b] [energy (eV)/f number]	Present results[a] [energy (eV)/f number]	Quantum-defect estimates[b] [energy (eV)/f number]
$(2\sigma_u)\,^1\Sigma_g^+ \rightarrow (ns\sigma_g)\,^1\Sigma_u^+$		$(2\sigma_g)\,^1\Sigma_g^+ \rightarrow (np\sigma_u)\,^1\Sigma_u^+$	
37.14/0.000 180	37.05/0.001 80	37.25/0.017 70	•••
39.22/0.000 002	39.22/0.000 50	45.42/0.000 0640	45.29/0.000 39
39.92/•••	39.93/0.000 20	46.70/0.000 0043	46.57/0.000 13
40.26/•••	40.25/0.000 11	47.19/0.000 0024	47.07/0.000 06
40.62/•••	40.43/0.000 06	47.45/0.000 0022	47.32/0.000 04
$(2\sigma_u)\,^1\Sigma_g^+ \rightarrow (nd\pi_g)\,^1\Pi_u$		$(2\sigma_g)\,^1\Sigma_g^+ \rightarrow (np\pi_u)\,^1\Pi_u$	
39.32/0.000 71	39.31/0.000 46	45.32/0.002 18	45.29/0.003 92
39.98/0.000 39	39.97/0.000 20	45.69/0.000 95	46.57/0.001 34
40.20/0.000 22	40.27/0.000 10	47.21/0.000 47	47.07/0.000 84
40.52/•••	40.44/0.000 06	47.48/•••	47.32/0.000 42

[a]As in Table III. Koopmans ionization potentials are employed.
[b]As in Table IV, employing quantum defects of $\delta = 1.1$, 0.0, 0.67, and 0.67, for $ns\sigma_g$, $nd\pi_g$, $np\sigma_u$, and $np\pi_u$ excitations for $n = 3, 4, \ldots$, respectively, and oscillator-strength densities at threshold of Fig. 4.

In contrast to the results of Fig. 3, the $3\sigma_g^{-1}$, $5\sigma^{-1}$, and $3\sigma_g^{-1}$ photoionization cross sections in N_2, CO, and O_2, respectively, have well-defined $\sigma \rightarrow k\sigma$ resonance features, rather than strong $N \rightarrow V_\sigma$ transitions below the ionization thresholds. It is apparently the case that the longer bond length in F_2 gives rise to a well-defined $(3\sigma_g^{-1}\sigma_u 2p)\,V_\sigma$ state below threshold, whereas the corresponding states appear in the photoionization continua in N_2, CO, and O_2.[1-4] These remarks are entirely in accord with the discussion of the $1\pi_g \rightarrow k\sigma_u$ spectra given above, in which case the $\sigma_u 2p$ valence orbital contributes only to the low-lying discrete $^1\Sigma_g^+ \rightarrow A\,^1\Pi_u$ transition (Table III), and not to the corresponding photoionization continuum. A more detailed description of $\sigma \rightarrow \sigma^*$ transitions in light diatomic molecules is given in a subsequent separate paper.

The calculated $3\sigma_g \rightarrow np\pi_u$ excitations of Table IV evidently constitute a Rydberg series in good accord with quantum-defect estimates using $\delta = 0.71$. The corresponding $3\sigma_g \rightarrow k\pi_u$ photoionization cross section has a well-defined resonancelike structure centered at 37 eV, ~5 eV above a presumably related peak in the $1\pi_g \rightarrow k\pi_u$ cross section of Fig. 2. The corresponding CO and O_2 profiles show somewhat related structures, although in these cases they are considerably broader.[2-4] This peak is conveniently regarded as a consequence of $3d$ atomic-fluorine pre-Rydberg orbitals that contribute substantially to the continuous spectrum, and, consequently, is given a $(3\sigma_g^{-1}\pi_u 3d)\,^1\Pi_u$ assignment. As in the case of the previously described resonances involving $3d$ atomic-orbital assignments, diabatic state calculations would be helpful in verifying the assignments.

D. $2\sigma_u$ (IP = 40.8 eV) and $2\sigma_g$ (IP = 47.9 eV) spectra

Although it is expected that the single-configuration frozen-core approximation will be less appropriate for ionization of the inner-valence $2\sigma_u$ and $2\sigma_g$ orbitals than for the outer-valence $1\pi_g$, $1\pi_u$, $3\sigma_g$ orbitals,[40] it is nevertheless of interest to present the calculated discrete and continuum spectra in these two cases. The reported static-exchange cross sections can be combined with appropriate photoelectron relative-intensity and curve-crossing calculations to obtain approximations for comparisons with experimental measurements of dissociative photoionization, when available.

In Table V and Fig. 4 are shown the discrete and continuum profiles, respectively, for the $2\sigma_u^{-1}$ and $2\sigma_g^{-1}$ channels. The positions of the $2\sigma_u \rightarrow ns\sigma_g$ and $nd\pi_g$ excitations evidently form Rydberg series with quantum defects of $\delta \cong 1.1$ and $\delta \cong 0$, respectively, whereas the positions of the $2\sigma_g \rightarrow np\pi_u$ and $np\sigma_u$ excitations form Rydberg series with $\delta \cong 0.67$ and $\delta \cong 0.67$, respectively. The intensities of the $2\sigma_u \rightarrow ns\sigma_g$ and $2\sigma_g \rightarrow np\sigma_u$ series differ substantially, however, from the quantum-defect estimates. This is perhaps due to the sensitivity of inner-valence-shell photoabsorption cross sections to the quality of description of the occupied orbital in the former case,[49,50] and perhaps due to the perturbing

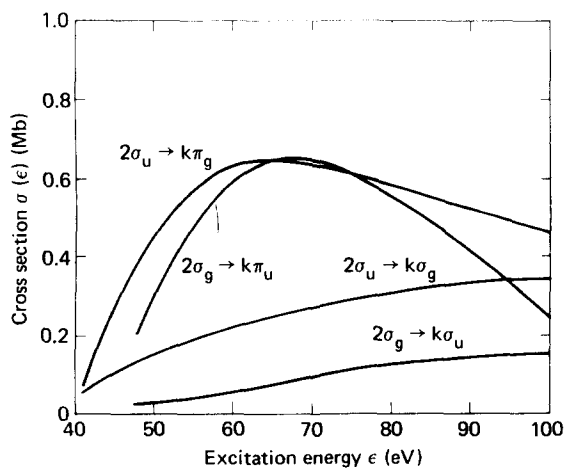

FIG. 4. As in Fig. 1, for $2\sigma_u \rightarrow k\sigma_g$ and $k\pi_g$ and $2\sigma_g \rightarrow k\sigma_u$ and $k\pi_u$ photoionization.

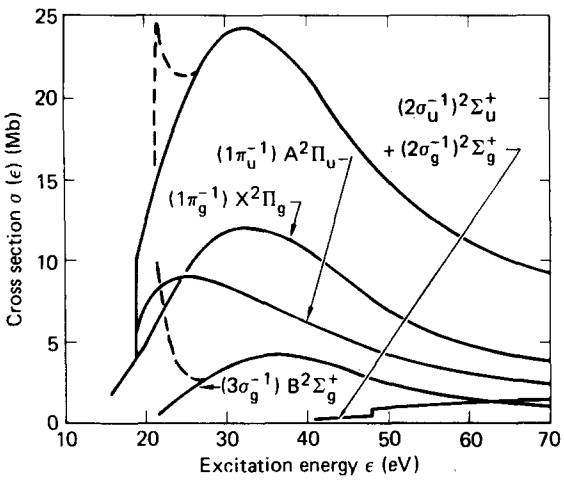

FIG. 5. Total photoionization and partial-channel photoionization cross sections in F_2 for production of $X^2\Pi_g$, $A^2\Pi_u$, $B^2\Sigma_g^+$, $(2\sigma_u^{-1})^2\Sigma_u^+$ and $(2\sigma_g^{-1})^2\Sigma_g^+$ parent F_2^+ ionic states. Dotted line as in Fig. 3.

$2\sigma_g \rightarrow \sigma_u 2p$ intravalence transition present in the latter case.

The photoionization cross sections shown in Fig. 4 are generally weak, and have shapes that are in general accord with expectations. Specifically, the $2\sigma_g \rightarrow k\sigma_u$ and $k\pi_u$ profiles are qualitatively similar to the $3\sigma_g \rightarrow k\sigma_u$ and $k\pi_u$ cross sections of Fig. 3, and the $2\sigma_u \rightarrow k\sigma_g$ and $k\pi_g$ profiles are similar to corresponding results in N_2.[1] Due to the sensitivity of inner-valence-shell photoionization cross sections to the quality of the occupied orbital employed,[49,50] basis-set refinements may result in cross sections that differ somewhat from those of Table V and Fig. 4.

E. Total cross section

The partial-channel $1\pi_g^{-1}$, $1\pi_u^{-1}$, $3\sigma_g^{-1}$, $2\sigma_u^{-1}$, and $2\sigma_g^{-1}$ photoionization cross sections obtained by summing the various symmetry contribution of Figs. 1–4 are shown in Fig. 5. Evidently, the cross section for formation of $(1\pi_g^{-1})\,X^2\Pi_g$ parent F_2^+ ions generally dominates, except at the lowest energies. The cross section for formation of $(1\pi_u^{-1})\,A^2\Pi_u$ parent F_2^+ ions is evidently the largest one at threshold, and that for production of $(3\sigma_g^{-1})\,B^2\Sigma_g^+$ parent ions is the smallest outer-valence-shell cross section. Note that the spurious contribution to the latter from the strongly perturbed Rydberg series is also shown in the figure as a dotted line for reference. Finally, the inner-valence-shell $2\sigma_u^{-1}$ and $2\sigma_g^{-1}$ cross sections are seen to be generally small, except at higher energy, where they should dominate the F^+ photoproduction process. It is, of course, important to recognize that the partial-channel cross sections of Fig. 5 refer to the production of parent F_2^+ ionic states. These states can contribute to production of F_2^+ ions, as well as to F^+ fragments arising from direct dissociation or appropriate curve crossings. Inspection of the calculated $X^2\Pi_g$, $A^2\Pi_u$, and $B^2\Sigma_g^+$ F_2^+ potential curves indicates the appropriate Franck–Condon regions are limited to narrow spectral intervals in the vibrationally discrete portions in these cases,[25] suggesting that the vertical electronic cross sections should be good approximations to vibrationally averaged results for formation of F_2^+ ions. Of course, it is possible that curve crossings can introduce somewhat more significant vibrational structures and lead to F^+ production, although in the absence of the necessary potential energy curves it is not possible to estimate these effects. The inner-valence $2\sigma_u^{-1}$ and $2\sigma_g^{-1}$ cross sections can be expected to contribute significantly to dissociative photoionization, as indicated above.

Also shown in Fig. 5 is the sum of the five partial-channel cross sections, giving the total vertical electronic photoabsorption–ionization cross section for the processes considered (Figs. 1–4). Since the various discrete states are not included in the total cross section, the result shown in these spectral regions correspond only to direct photoionization, and do not include autoionization. In those spectral regions in which direct one-electron photoionization dominates, the results shown correspond to total absorption, resulting in the production of both F_2^+ ions and F^+ fragments, as indicated above. There are apparently no corresponding experimental studies available for comparison with the results of Fig. 5 at this time.[51]

V. CONCLUDING REMARKS

The present studies in the static-exchange approximation provide the basis for an overall quantitative account of outer- and inner-valence-shell photoexcitation and ionization in molecular fluorine. Because the Stieltjes–Tchebycheff approach employed treats the discrete and continuous portions of the photoabsorption cross section from a common perspective, it is possible to account for the various structures appearing in the calculated static-exchange partial-channel cross sections in terms of conventional molecular-orbital models. Specifically, the discrete excitation spectra are found to be comprised of various Rydberg series, and of intravalence transitions involving final-state compact $\sigma_u 2p$ virtual orbitals and corresponding V_σ states. The photoionization continua exhibit resonancelike structures that can be attributed to contributions from pre-Rydberg atomic orbitals to the $k\pi_u$, $k\delta_u$, and $k\delta_g$ final-state spectra. Specifically, it is suggested that $(1\pi_g^{-1}\pi_u 3d)\,^1\Sigma_u^+$, $(1\pi_g^{-1}\delta_u 3d)\,^1\Pi_u$, $(1\pi_u^{-1}\delta_g 3d)\,^1\Pi_u$, and $(3\sigma_g, \pi_u 3d)\,^1\Pi_u$ diabatic states correlating with the dipole-allowed $(2p^{-1}3d)\,^2D^e$ atomic-fluorine state cross the outer limbs of appropriate Rydberg series and corresponding ionic-state-potential curves, appearing as photoionization resonances at the ground-state equilibrium internuclear separation. Although this interpretation is a plausible one, appropriate diabatic state calculations are recommended for additional clarification.

The various discrete and continuum features in the F_2 spectrum are in general accord with the corresponding related cross sections obtained from previously reported studies in N_2, CO, and O_2. The one major difference among the spectra is rather significant, how-

ever. As indicated above, there is a well-defined $N \rightarrow V_\sigma$ or $3\sigma_g \rightarrow 3\sigma_u\,(\sigma_u 2p)$ transition below the $3\sigma_g$ ionization threshold in F_2, whereas this feature appears as a broad resonance in the $3\sigma_g \rightarrow k\sigma_u$ photoionization continua in N_2 and O_2, and in the $5\sigma \rightarrow k\sigma$ cross section in CO. The origin of this significant difference between the dipole spectra in N_2, CO, and O_2 on the one hand, and in F_2 on the other, can be attributed to the longer bond length in F_2, allowing the σ^* orbital to assume a position below the ionization potential in this case, whereas the shorter bond lengths in N_2, CO, and O_2 force the corresponding σ^* orbitals above the appropriate ionization potentials.

Although more elaborate calculations, including channel-coupling effects, consideration of the vibrational degrees of freedom, and basis-set refinements, will presumably change somewhat the quantitative aspects of the cross sections reported here, the general nature of the spectrum and the qualitative interpretation of the results in terms of molecular-orbital concepts are likely to be invariant to these refinements.

ACKNOWLEDGMENTS

Acknowledgment is made to the National Science Foundation for support provided to B. V. M., and to the Donors of the Petroleum Research Fund, administered by the American Chemical Society, and to the National Research Council, for providing support to P. W. L. The kind hospitality of J. O. Arnold and S. R. Langhoff of the NASA–Ames Research Center Computational Chemistry Group, and of D. Bershader of the Department of Aeronautics and Astronautics, Stanford University, to P.W.L. is also gratefully acknowledged. The work of T.N.R. and A.E.O. was performed under the auspices of the U.S. Energy Research and Development Administration under Contract No. W-7405-Eng-48.

[1]T. N. Rescigno, C. F. Bender, B. V. McKoy, and P. W. Langhoff, J. Chem. Phys. **68**, 970 (1978).
[2]N. Padial, G. Csanak, B. V. McKoy, and P. W. Langhoff, J. Chem. Phys. **69**, 2992 (1978).
[3]A. Gerwer, C. Asaro, B. V. McKoy, and P. W. Langhoff, J. Chem. Phys. **72**, 713 (1979).
[4]P. W. Langhoff, A. Gerwer, C. Asaro, and B. V. McKoy, Int. J. Quantum Chem. **S13**, 645 (1979).
[5]P. W. Langhoff, in *Electron–Molecule and Photon–Molecule Collisions*, edited by T. N. Rescigno, B. V. McKoy, and B. Schneider (Plenum, New York, 1979), pp. 183–224.
[6]A. Lofthus and P. H. Krupenie, J. Phys. Chem. Ref. Data **6**, 113 (1977).
[7]P. H. Krupenie, Natl. Stand. Ref. Data Ser. Natl. Bur. Stand. **5** (1966).
[8]P. H. Krupenie, J. Phys. Chem. Ref. Data **1**, 423 (1972).
[9]R. L. Blake and J. H. Carver, J. Chem. Phys. **47**, 1038 (1967).
[10]L. C. Lee, R. W. Carlson, D. L. Judge, and M. Ogawa, J. Quant. Spectrosc. Radiat. Transfer **13**, 1023 (1973).
[11]J. A. R. Samson and J. L. Gardner, J. Electron Spectrosc. Relat. Phenom. 8, 35 (1976).
[12]A. Hamnett, W. Stoll, and C. E. Brion, J. Electron Spectrosc. Relat. Phenom. **8**, 367 (1976).
[13]G. R. Wight, M. J. Van der Wiel, and C. E. Brion, J. Phys. B **9**, 675 (1976).
[14]P. R. Woodruff and G. V. Marr, J. Phys. B **9**, L377 (1976); Proc. R. Soc. London A **358**, 87 (1977).
[15]E. W. Plummer, T. Gustafsson, W. Gudat, and D. E. Eastman, Phys. Rev. A **15**, 2339 (1977); T. Gustafsson (private communications).
[16]J. A. R. Samson, G. N. Haddad, and J. L. Gardner, J. Phys. B **10**, 1749 (1977).
[17]J. A. R. Samson, J. L. Gardner, and G. N. Haddad, J. Electron Spectrosc. Relat. Phenom. **12**, 281 (1977).
[18]G. Mehlman, D. L. Ederer, and E. B. Saloman, J. Chem. Phys. **68**, 1862 (1978).
[19]C. E. Brion, K. H. Tan, M. J. van der Wiel, and Ph. E. van der Leeuw, J. Electron Spectrosc. Relat. Phenom. **17**, 101 (1979).
[20]D. A. Vroom, D. C. Frost, and C. A. McDowell, J. Chem. Phys. **46**, 4255 (1967).
[21]A. B. Cornford, D. C. Frost, C. A. McDowell, J. L. Ragle, and I. A. Stenhouse, J. Chem. Phys. **54**, 2651 (1971).
[22]A. W. Potts and W. C. Price, Trans. Faraday Soc. **67**, 1242 (1971); W. C. Price, Phys. Bull. **23**, 87 (1972).
[23]J. L. Gole and J. L. Margrave, J. Mol. Spectrosc. **43**, 65 (1972).
[24]E. A. Colbourn, M. Dagenais, A. E. Douglas, and J. W. Raymonds, Can. J. Phys. **54**, 1343 (1976).
[25]P. E. Cade and A. C. Wahl, J. Chem. Phys. **41**, 2600 (1964); At. Data **13**, 399 (1974).
[26]P. J. Hay and D. C. Cartwright, Chem. Phys. Lett. **41**, 80 (1976); **42**, 398 (1976).
[27]D. Demoulin and M. Jungen, Chem. Phys. **16**, 311 (1976).
[28]T. N. Rescigno, C. F. Bender, and B. V. McKoy, Chem. Phys. Lett. **45**, 307 (1977).
[29]D. C. Cartwright and P. J. Hay, J. Chem. Phys. **70**, 3191 (1979); C. F. Bender (private communication).
[30]H. F. Schaefer, III, *The Electronic Structure of Atoms and Molecules* (Addison-Wesley, Reading, MA, 1972).
[31]T. H. Dunning and P. J. Hay, in *Modern Theoretical Chemistry*, edited by H. F. Schaefer, III (Plenum, New York, 1976), Vol. 3, Chap. 1.
[32]P. W. Langhoff, Chem. Phys. Lett. **22**, 60 (1973).
[33]P. W. Langhoff and C. T. Corcoran, J. Chem. Phys. **61**, 146 (1974).
[34]P. W. Langhoff, J. Sims, and C. T. Corcoran, Phys. Rev. A **10**, 829 (1974).
[35]P. W. Langhoff and C. T. Corcoran, Chem. Phys. Lett. **40**, 367 (1976).
[36]P. W. Langhoff, C. T. Corcoran, J. S. Sims, F. Weinhold, and R. M. Glover, Phys. Rev. A **14**, 1042 (1976).
[37]C. T. Corcoran and P. W. Langhoff, J. Math. Phys. **18**, 651 (1977).
[38]H. Lefebvre-Brion, C. M. Moser, and R. K. Nesbet, J. Chem. Phys. **35**, 1702 (1961); P. W. Langhoff, M. Karplus, and R. P. Hurst, J. Chem. Phys. **44**, 505 (1966); W. J. Hunt and W. A. Goddard, Chem. Phys. Lett. **3**, 414 (1969); **24**, 464 (1974).
[39]R. S. Mulliken and W. C. Ermler, *Diatomic Molecules* (Academic, New York, 1977).
[40]J. Schirmer, L. S. Cederbaum, W. Domcke, and W. von Niessen, Chem. Phys. **26**, 149 (1977).
[41]E. U. Condon and G. H. Shortley, *The Theory of Atomic Spectra* (Cambridge University, Cambridge, London, 1963), p. 98.
[42]G. Herzberg, *Spectra of Diatomic Molecules*, 2nd ed. (Van Nostrand, New York, 1950).
[43]P. A. Cox and F. A. Orchard, Chem. Phys. Lett. **7**, 273 (1970).
[44]O. Sinanoğlu, in *Chemical Spectroscopy and Photochemistry in the Vacuum Ultraviolet*, edited by C. Sandorfy, P. J. Ausloss, and M. B. Robin (Reidel, Boston, MA, 1974), pp. 337–384.

[45]R. J. Buenker and S. D. Peyerimhoff, Chem. Phys. Lett. **34**, 225 (1975); Chem. Phys. **8**, 324 (1975).
[46]C. E. Moore, *Atomic Energy Levels*, U.S. Natl. Bur. Stand. Circ. No. 467 (U. S. GPO, Washington, D.C., 1949), Vol. 1.
[47]T. N. Rescigno, A. Gerwer, B. V. McKoy, and P. W. Langhoff, Chem. Phys. Lett. **66**, 116 (1979).
[48]E. Lindholm, Ark. Fys. **40**, 111 (1969).
[49]K. Faegri, Int. J. Quantum Chem. **15**, 411 (1979).
[50]R. L. Martin, W. R. Daasch, and E. R. Davidson, J. Chem. Phys. **71**, 2375 (1978).
[51]We are informed by C. E. Brion (private communication) that experimental studies are presently contemplated.